

**Reduction in oxidative stress during cellular responses to chemically functionalised graphene**

Journal:	<i>Journal of Materials Chemistry B</i>
Manuscript ID:	TB-ART-03-2014-000478.R1
Article Type:	Paper
Date Submitted by the Author:	10-Jun-2014
Complete List of Authors:	Lee, Nae_Eung; Sungkyunkwan, Advanced Materials Science and Engineering Yoon, Ok-Ja; Sungkyunkwan University, Advanced Materials Science and Engineering; Chung-Ang University, Department of Chemistry Jung, Chang; Sungkyunkwan University, Advanced Materials Science and Engineering Sohn, Il; Sungkyunkwan University, Advanced Materials Science and Engineering Son, Young; Sungkyunkwan University, Advanced Materials Science and Engineering Hwanga, Byeong-Ung; Sungkyunkwan University, Advanced Materials Science and Engineering Kim, Il; Sungkyunkwan University, Advanced Materials Science and Engineering

Cite this: DOI: 10.1039/c0xx00000x

www.rsc.org/xxxxxx

ARTICLE TYPE

## Reduction in oxidative stress during cellular responses to chemically functionalised graphene

Ok Ja Yoon,<sup>a,d,‡</sup> Chang Yong Jung,<sup>a,‡</sup> Il Yung Sohn,<sup>a</sup> Young Min Son,<sup>b</sup> Byeong-Ung Hwang,<sup>a</sup> Il Jin Kim,<sup>a</sup> and Nae-Eung Lee,<sup>\*a,b,c</sup>

<sup>5</sup> Received (in XXX, XXX) XthXXXXXXXXXX 20XX, Accepted Xth XXXXXXXXXXXX 20XX

DOI: 10.1039/b000000x

The two-dimensional nanocarbon material graphene (Gr) has been extensively studied due its many potential biomedical applications including regenerative medicine, drug delivery, bioimaging, and biosensing. The effects of nitrogen-functionalisation on chemically-driven Gr (CDG) cellular responses were studied by investigating the generation of reactive oxygen species (ROS) and mitochondrial morphology as well as focal adhesion, shape, proliferation and viability of HeLa cells grown on functionalised CDG (*f*-CDG) films. The drop casting of CDG nanosheets formed thin CDG films and the formation of nitrogen groups on the *f*-CDG thin films was mediated by N<sub>2</sub> plasma treatment without the formation of observable surface defects. N-containing functional groups on the CDG thin films contributed to an increase in hydrophilicity. The proliferation and viability of HeLa cells grown on the *f*-CDG thin films were enhanced compared to those grown on CDG films alone and control samples. N-functionalisation of CDG thin films effectively reduced the ROS generated from cells on the *f*-CDG films. These results indicate that N<sub>2</sub> plasma treatment of CDG is very useful in improving biocompatibility for the bio-application of graphene materials.

### Introduction

Graphene (Gr) due to its excellent physicochemical, electrical and mechanical properties has recently been reported as useful for a variety of biomedical applications<sup>1-3</sup> including biosensing,<sup>4</sup> bioimaging,<sup>5, 6</sup> anticancer therapy,<sup>7, 8</sup> tissue engineering as scaffolds,<sup>9</sup> and drug delivery systems (DDS).<sup>8, 10-12</sup> Some research has also demonstrated the potential application of Gr for stem cell research.<sup>10, 11</sup> The most important parameters for the use of Gr in anticancer therapies and DDS include size, charge state, and surface functional groups that affect biological and toxicological aspects of Gr.<sup>8</sup> The Gr-based scaffolds for regenerative medicine indicate some degree of biocompatibility for adhesion, growth, differentiation and proliferation of cells *in vitro*.<sup>10</sup> However, Wang et al. reported that mammalian cell growth was not promoted on a Gr substrate compared to cell growth on a graphene oxide (GO) substrate.<sup>13</sup> These previous research results indicate that the surface chemical properties of Gr affect cellular responses, and the mechanism that mediates growth inhibition needs to be elucidated. Therefore, the biocompatibility of Gr materials for subsequent improvement of biomedical applications needs more detailed investigation.

To improve biocompatibility and reduce Gr cytotoxicity, Gr is often covalently functionalised using novel, biocompatible materials such as poly-L-lysine (PLL), chitosan, and dextrin.<sup>14-16</sup> Many studies have focused on the improvement of Gr and carbon nanotube (CNT) hydrophilicity through the formation of functional groups on Gr and CNTs to control surface charge and surface energy in order to promote the interaction between cells and nanocarbon scaffolds.<sup>17</sup> Surface functionalisation of

nanocarbon materials by plasma surface treatment is very useful in generating various functional groups related to bio-affinity properties (e.g., carboxyl and hydroxyl groups as negative charges and nitrogen and amine groups as positive charges).<sup>18, 19</sup> An important potential advantage of using plasmas is the production of reactive species that enhance surface chemical reactions for the purpose of surface modification on scaffolds. The resulting modification of surface chemical properties reduces the generation of reactive oxygen species (ROS) and reactive nitrogen species (RNS) during cell growth and, as a result, influences cell proliferation and viability.<sup>20, 21</sup> We previously investigated enhancement of neuronal environments by studying the interactions between neuronal cells with single-walled CNTs functionalised by O<sub>2</sub><sup>22</sup> and N<sub>2</sub> plasma<sup>23</sup> treatments. However, the effects of Gr surface functional groups on intracellular ROS levels and cytotoxicity have not been investigated in detail.

It is well known that exposure of nanoscale materials to cells often produces a high level of ROS causing cell apoptosis.<sup>24, 25</sup> ROS such as superoxide anion (O<sub>2</sub><sup>-</sup>) and hydrogen peroxide (H<sub>2</sub>O<sub>2</sub>) are generated during aerobic metabolism<sup>26</sup> and play important roles in cell signalling and homeostasis.<sup>27</sup> Also, the source of ROS is from mitochondrial damage; therefore, analysis of mitochondrial morphology is very important in order to understand ROS generation.<sup>28</sup>

Herein, we studied oxidative stress by investigating ROS generation, mitochondrial morphology, focal adhesion, cell shape, proliferation and viability of HeLa cells grown on untreated chemically driven graphene (CDG) and functionalised CDG (*f*-CDG) thin films. Functionalisation of the CDG thin

films was obtained by N<sub>2</sub> plasma treatments while the defect generation on the treated CDG films was suppressed. Because HeLa cells can produce considerable amounts of H<sub>2</sub>O<sub>2</sub> without exogenous stimulation, the oxidative stress of HeLa cells grown on both CDG and *f*-CDG thin films could be investigated and compared. The results indicate that the nitrogen-containing functional groups on *f*-CDG thin films significantly reduce oxidative stress and cytotoxicity during cell growth compared to cell growth on untreated CDG thin films.

## Results and Discussion

### Characteristics of CDG and *f*-CDG thin films

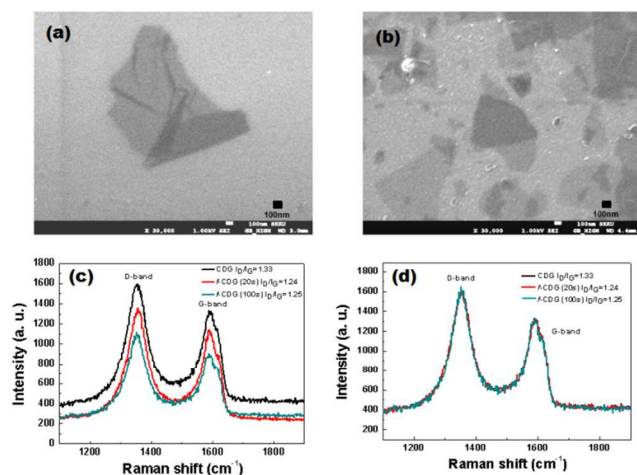


**Fig. 1** FE-SEM images of (a) CDG and (b) *f*-CDG nanosheets treated by N<sub>2</sub> plasma for 100 s. Micro-Raman spectra of (c) CDG and *f*-CDG (20 and 100 s) samples. (d) Normalisation of micro-Raman spectra.

To investigate the effects of N<sub>2</sub> plasma treatment on the morphological and chemical properties of the CDG thin films, we prepared untreated and N<sub>2</sub> plasma-treated samples (treatment time of 20 and 100 s), denoted as CDG, *f*-CDG (20 s) and *f*-CDG (100 s), respectively. For clear observation of morphological changes in CDG nanosheets after the plasma treatments, the CDG nanosheets were placed on a cover slip without formation of a thin film. The comparison of the CDG and *f*-CDG (100 s) nanosheet surfaces in Figs. 1a, b shows no significant observable change in their morphology after N<sub>2</sub> plasma treatment.

The micro-Raman spectra of untreated and plasma-treated CDG thin films (Fig. 1c) also confirmed damage-free surfaces after plasma treatment. The intensity ratios, I<sub>D</sub>/I<sub>G</sub>, of the 1,349 cm<sup>-1</sup> wave number, which corresponds to the disorder-induced D mode, and the 1,590 cm<sup>-1</sup> wave number, which corresponds to the C-C stretching G mode, were 1.33, 1.24, and 1.25 for CDG, *f*-CDG (20 s), and *f*-CDG (100 s) thin films, respectively. The average I<sub>D</sub>/I<sub>G</sub> values of twenty point measurements from three samples were about 1.1 (Supporting Fig. S1). The normalised Raman spectra in Fig. 1d indicated no significant difference between those of the CDG and *f*-CDG thin films. No shift in the G-band from *f*-CDG (20 and 100 s) samples compared to the CDG sample in this experiment indicates the generation of no topological defects within the instrumental detection limit. Down shifts of the G-band due to N-doping of Gr by the thermal and plasma treatments, similar to that of the N-doped CNTs, were often observed in the case formation of topological defects.<sup>29, 30</sup>

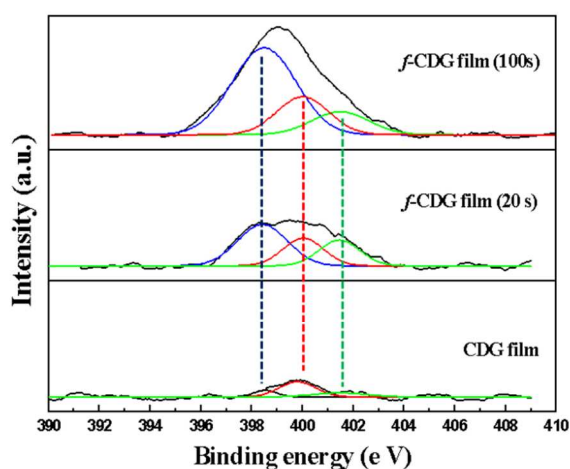


**Fig. 2** N1s XPS spectra of (a) CDG, (b) *f*-CDG (20 s), (c) *f*-CDG (100 s)

In order to investigate the changes in chemical properties of plasma-treated CDG thin films, X-ray photoelectron spectroscopy (XPS) measurements of the untreated and treated samples were carried out. Three N 1s XPS spectra were obtained from each sample. The N-binding components on the CDG, *f*-CDG (20 s), and *f*-CDG (100 s) thin films of 1.5, 3.4, and 5.8%, respectively (Supporting Table S1), were shown in the Fig. 2. The average N-binding components on the CDG, *f*-CDG (20 s), and *f*-CDG (100 s) thin films were 2.6, 3.6, and 6.5%, respectively (Supporting Fig. S2). The CDG sample showed a low N-binding component due to remained residues after the chemical reduction by hydrazine vapor but the N-binding components of the *f*-CDG (20 and 100 s) thin films increased with plasma-treatment time. The N 1s spectra of the CDG and *f*-CDG (20 and 100 s) thin films in Fig. 2 contains three distinctive peaks of pyridinic N (398.5 eV), pyrrolic N (400.2 eV) and graphitic N (401.5 eV), respectively.<sup>31</sup> The component ratios shown in Supporting Information (Table S2) were obtained from N1s spectra in Fig. 2. The XPS data in Fig. 2 and Table S2 clearly indicate the increased pyridinic N (six-member ring) formation of N-containing functional groups on the surface of the CDG by plasma treatments. The increase in pyridinic N components may be attributed to binding of reactive N species in the plasma to the edge and defects of CDG planes.

The contact angles of the treated and untreated samples were measured to characterise the surface properties of plasma-treated CDG samples. The contact angle values of 62°, 33°, and 28° were obtained for CDG, *f*-CDG (20 s), and *f*-CDG (100 s) thin films, respectively. The surfaces of *f*-CDG thin films were more hydrophilic due to the enhanced positively charged polar groups in the increased pyridinic N (six-member ring) in N-containing functional groups compared to the CDG thin film. Hydrophilicity of *f*-CDG thin films is expected to affect oxidative stress, focal adhesion, proliferation and viability in cellular responses to *f*-CDG.

### Analysis of cell morphology and focal adhesion

To investigate the effects of CDG functionalisation on cellular responses, cell morphologies were characterised for cells grown on a bare coverslip, CDG, and *f*-CDG thin films. Fluorescence cell images were obtained using an inverted microscope to detect

vinculin, a membrane-cytoskeletal protein in the focal adhesion plaques associated with cell-cell and cell-matrix junctions<sup>32</sup> (green fluorescent images in the left column of Figs. 3a-d). In addition, mitochondrial morphologies were investigated in cells grown on a bare coverslip, CDG, and *f*-CDG thin films (red fluorescent images in the right column of Figs. 3a-d) and CSLM (the inserts in the right column of Figs. 3a-d). Vinculin is associated with the focal adhesion of cells and the adherent

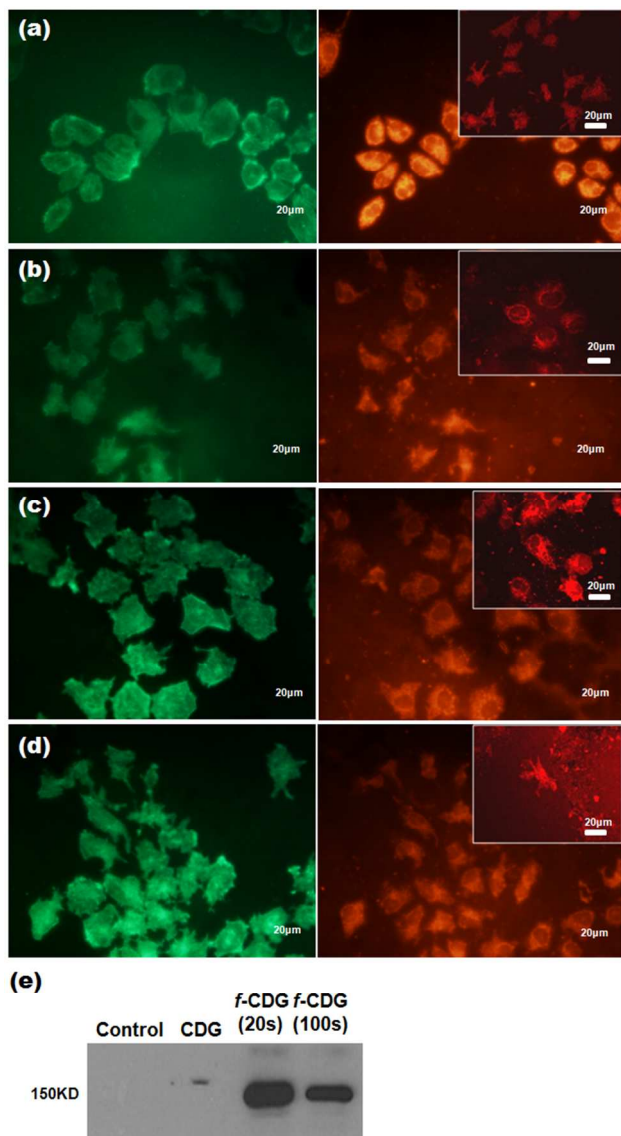


**Fig. 3** Fluorescence images of vinculin (left column) and mitochondrial morphology (right column) from HeLa cells grown on (a) a bare coverslip, (b) CDG, (c) *f*-CDG (20 s), and (d) *f*-CDG (100 s) thin films. The fluorescence images of vinculin and mitochondria were obtained using an inverted optical microscope (magnified to 400x). The inserts are mitochondrial morphologies obtained by Vis CLSM (magnified to 400x). (e) Western blot of vinculin production.

junction is able to interact with the cytoskeleton to control cell shape, cell spreading, and lamellipodia formation.<sup>33</sup> HeLa cells grown on the bare coverslip (Fig. 3a), CDG (Fig. 3b), and *f*-CDG (Figs. 3c-d) thin films appeared to assemble at focal adhesions and actin stress fibres with cytoskeletal tubulin. In particular, lamellipodia formation on the *f*-CDG thin films (Figs. 3c-d)

showed more abundance and remarkable difference from that seen in cells grown on a bare coverslip (Fig. 3a) and CDG thin films (Fig. 3b); therefore, strong focal adhesion and cell spreading were formed on the *f*-CDG thin films (Figs. 3c-d). Cell shapes that are controlled by a complex interaction with the cytoskeleton and extracellular matrix were influenced by the proliferation and focal adhesions.

The mitochondrial morphologies of cells grown on *f*-CDG thin films obtained by the fluorescence microscopy (see the left column of Figs. 3c, d) and by confocal laser scanning microscope (CLSM) (see the inserts in Figs. 3c, d) indicated that a filamentous network with increased interconnected tubular shape due to fusion mixed with a short and small spherical shape was formed. In addition, mitochondrial fragmentation was decreased compared to cells grown on a bare coverslip and CDG thin film (see the inserts in Figs. 3a, b). Mitochondria play a critical role in cellular energy metabolism by producing adenosine 5'-triphosphate (ATP) and many other cellular processes including programmed cell death by the production of ROS.<sup>34</sup> Due to their diverse functions, mitochondria present with a range of morphologies, including small spheres and interconnected tubules.<sup>35</sup> These changes in mitochondrial morphology occur during cell division.<sup>36, 37</sup> Higher ROS in the CDG sample might have caused an important contribution to oxidative stress or damage resulting in the short and small spherical shape; as a result, the fragmented mitochondria are generated by fission.<sup>38</sup> The observed morphological differences of mitochondria indicate less ROS generation from the cells grown on *f*-CDG thin films (20 s) compared to those grown on *f*-CDG thin films (100 s).

Vinculin production level was analysed by Western blotting methods after cell culturing for 24 h (Fig. 3e). The difference in vinculin production level in Fig. 3e shows strong staining and higher levels of activated cytoskeleton components in cells grown on the *f*-CDG thin films compared to those grown on a bare coverslip or the CDG thin film. These results demonstrate enhanced adhesion and spreading of the cells on *f*-CDG films due to improved scaffolding capabilities. Increased vinculin production levels from cells grown on the *f*-CDG (20 s) sample compared to that of the CDG thin film indicates a slightly increased level of cell adhesion and spreading ability of cells on the *f*-CDG (20 s) thin film. However, lower vinculin production levels from cells grown on the *f*-CDG (100 s) thin film than those grown on the *f*-CDG (20 s) film is consistent with lower lamellipodia formation levels associated with vinculin observed in the fluorescence images (Figs. 3c-d) but indicates slightly inhibited focal adhesion and reduced polymerisation of actin filaments.

#### ROS generation of cells on CDG and *f*-CDG thin films

ROS generation has been widely used to assess toxicological mechanisms.<sup>39</sup> Therefore, we must consider the oxidative stress of cells grown on CDG and *f*-CDG thin films for biocompatibility as scaffold materials.<sup>20, 21</sup> The DCF-DA stained HeLa cells were analysed by flow cytometry and the data are shown in Fig. 4. The count vs. fluorescein isothiocyanate A (FITC-A) plots of Figs. 4a-e present the ROS level in stressed cells by apoptosis. P1 indicates the cell numbers in the polygon gate by side scatter-area (SSC-A) vs. forward scatter-area (FSC-A) plots in Supporting

Figure S3. The P2 and P3 channels were designated as positive events. The positive control for ROS level after exposure to 100  $\mu\text{M}$   $\text{H}_2\text{O}_2$  and the negative control for ROS level of cells on a bare coverslip were both included in the analysis. The ROS level in cells grown on *f*-CDG (20 s) thin films (P3: 40.8%) was decreased compared to those on CDG (P3: 46.9%) and *f*-CDG (100 s) (P3: 62.2%) thin films. The ROS level in cells grown on the *f*-CDG (20 s) thin films was slightly increased relative to that in the negative control. Since ROS damage changed mitochondrial morphology, reduced oxidative stress of cells on the *f*-CDG (20 s) thin film with lower ROS levels was associated with relatively less change in mitochondrial morphology compared to cells on the CDG film and *f*-CDG (100 s) thin films observed in Fig. 3.

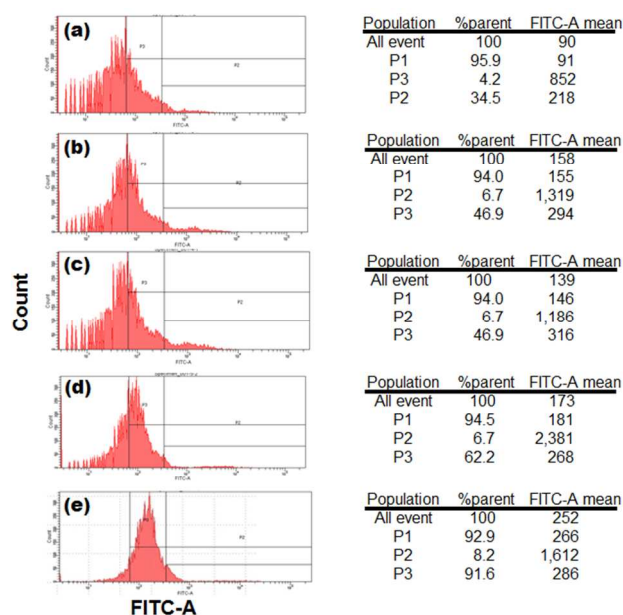


Fig. 4 Flow cytometry analysis of ROS generation by count vs. FITC-A plots on the (a) negative control, (b) CDG, (c) *f*-CDG (20 s), (d) *f*-CDG (100 s) thin films, and (e) positive  $\text{H}_2\text{O}_2$  (100  $\mu\text{M}$ ) plots, respectively.

#### Analysis of cell proliferation and viability

To evaluate the biocompatibility of CDG and *f*-CDG thin films, the proliferation and viability of HeLa cells cultured for two days on CDG and *f*-CDG films in 24-well plates were measured via the optical water-soluble tetrazolium salt-1 (WST-1) assay. The WST-1 assay results shown in Fig. 5 demonstrate increased proliferation and viability of the cells grown on the *f*-CDG thin film (20 s) compared to the cells grown on a bare coverslip (control), CDG thin film, and *f*-CDG thin film (100 s). Proliferation and viability of the cells on the CDG and *f*-CDG (100 s) thin films were clearly decreased compared to that of the cells grown on the CDG thin film (20 s). The *f*-CDG (20 s) film with lower hydrophilicity than *f*-CDG (100 s) film showed reduced oxidative stress and improved cell shape, increased focal adhesion, and enhanced proliferation and viability of cells even though the reason was not clearly understood from the present experiments. It was reported that fibroblast cellular adhesion strength and proliferation were increased on polymer materials of low surface energy more than high surface energy

such as metal materials associated with increased large surface roughness.<sup>40</sup> These combined results of cell and mitochondrial morphological observation, Western blot analysis, ROS measurements, and cell viability and proliferation analysis indicate that the *f*-CDG (20 s) thin films provide greater potential for application as a scaffold material due to enhanced biocompatibility and bio-affinity compared to the CDG thin film and *f*-CDG (100 s) thin film.

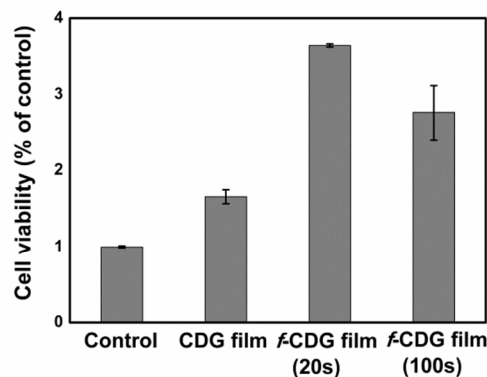


Fig. 5 Cell viability and proliferation by WST-1 analysis

## Experimental

### Preparation of CDG thin films

GO nanosheet powder was synthesised by a modified Hummers method from purified natural graphite flakes (purchased from Sigma Aldrich).<sup>11</sup> A solution of GO nanosheets was prepared by mixing GO nanosheet powder (6.0 mg) and deionised water (2.0 ml) followed by ultrasonication for 2 h. Then, *N,N'*-dimethylformamide (DMF, 99.5%, Junsei, Tokyo, Japan) solvent (15 ml) and hydrazine hydrate solution (24–26%, Sigma Aldrich, 1.0 ml) was added to the solution by mixing. The mixed solution was stirred for 24 h at 90 °C for reduction and washed with ethanol at room temperature. After reduction of the GO nanosheets in solution by hydrazine hydrate, the CDG nanosheet powder was obtained by heating the solution dropped on Teflon film at 80 °C.

Next, dispersion of the CDG nanosheets was achieved with a mixture of ethyl alcohol solvent, which resulted in a 10 mg/ml concentration of CDG powder. The CDG nanosheet solution was further mixed by magnetic stirring for 2h. The CDG thin films with a thickness of  $\sim 5.0$   $\mu\text{m}$  were formed on a coverslip (diameter; 12 mm, thickness; 0.13–0.17 mm) by drying at 80 °C after drop casting 0.5 ml of the prepared CDG solution.

### Surface functionalisation of CDG thin films

To obtain *f*-CDG thin films, the surface of the CDG thin films on the coverslip was treated by  $\text{N}_2$  plasma for functionalisation. The plasma treatment was performed in a plasma reactor equipped with a dome-shaped radio-frequency (RF) electrode on top of the reactor, and  $\text{N}_2$  gas was directly injected into the reactor through a quartz injector. The RF electrode was powered by a 13.56 MHz RF power source with an input power of 1 kW. The working pressure was fixed at 1 Torr and a  $\text{N}_2$  flow rate of 200 sccm was used for nitrogen functionalisation. A throttle valve controlled the chamber pressure. Treatment times of 20 and 100 s

were used.

#### CDG and *f*-CDG thin film analytical methods

The surfaces of the CDG and *f*-CDG thin films were characterised by XPS (ESCA2000, VG Microtec). For XPS sample preparation, the plasma-treated films on a 12 mm coverslip were transferred to carbon tape. The XPS spectra were obtained with non-monochromatic Al K $\alpha$  radiation (195 W) in the wide scan (0–1000 eV) using a pass energy of 20 eV. The core-level signals were obtained at a photoelectron take-off angle of 54.7°. All spectra were referenced to the hydrocarbon C 1s peak at a binding energy of 285 eV. The spectrum analysis was carried out by fitting the peak shape using Lorentzian transformation. Measurements were performed in triplicate, and the measured data are shown with standard deviations.

The micro-Raman spectra of the CDG and *f*-CDG thin films were obtained under ambient conditions using the 514.5 nm line of an argon ion laser. The Raman measurements were performed using backscattering geometry with a JY LabRam HR fit with a liquid-nitrogen cooled charge-coupled device detector. Measurements of twenty points were performed and the measured data are shown with standard deviations.

The surface morphologies of the CDG and *f*-CDG thin films were measured using field-emission scanning electron microscopy (FE-SEM; JSM 890, JEOL Ltd.). A contact anglemeter (Phoenix 300, Surface Electro Optics Co. Ltd.) was employed to measure the contact angles of deionised water on the CDG and *f*-CDG thin films.

#### Cell culture

HeLa cells were purchased from the Korea Cell Line Bank (Seoul, Korea). These cells were cultured in Roswell Park Memorial Institute (RPMI) medium supplemented with 10% heat-inactivated fetal bovine serum (FBS) along with a 1% (vol/vol) antibiotic mixture (Invitrogen) in a 95 % humidified air and 5% CO<sub>2</sub> atmosphere at 37 °C. After reaching about 80% confluency, cells were subcultured by trypsinisation. Cells were plated with a density of 4x10<sup>5</sup> per well and grown for two days on CDG and *f*-CDG films formed on coverslips placed inside of the wells of 24-well plates.

#### HeLa cell morphological analyses

For immunofluorescence microscopy, HeLa cells at 1x10<sup>3</sup> per well were grown on coverslips with CDG and *f*-CDG thin films in Dulbecco's Modified Eagle Medium (DMEM) supplemented with 10% (vol/vol) FBS, 2.0 mM glutamine, 100 U/ml penicillin, and 100 µg/ml streptomycin (Cellgro, Corning) in 5% CO<sub>2</sub> at 37 °C. Cells were pre-incubated in serum free DMEM for 3 h and then incubated in the presence of 100 nM Mito Tracker Red CMXRos dye (Life Technologies Corp.) for 45 min in 5% CO<sub>2</sub> at 37 °C. Then, after washes with phosphate buffered saline (PBS), the cells were fixed in 4% paraformaldehyde (PFA) for 30 min at room temperature (RT) and permeabilised with 0.05% saponin in PBS for 15 min. After permeabilisation, cells were blocked with PBS containing 1% bovine serum albumin (BSA) for 30 min and incubated with Alexa Fluor-488 Phalloidin (Life Technologies Corp.) in PBS containing 1% BSA for 2h at RT. Then, cells were washed in triplicate with PBS and subsequently mounted using

Vectashield (Vector Laboratories, Inc.). Fluorescence images were acquired using an inverted optical microscope (IX71, Olympus Inc., Ltd)]. Fluorescence images of vinculin, a membrane skeleton protein, were obtained using an inverted optical microscope via excitation of Alexa Fluor 488. Mitochondrial morphologies were obtained using an inverted optical microscope and a visible CLSM (LSM 510 META, Carl Zeiss AG, Jena, Germany). The 579 nm line of a He-Ne laser with a 533-633nm band pass filter was used for the excitation of MitoTracker Red CMXRos in CLSM.

#### Analysis of ROS generation

For intracellular ROS analysis, cultured cells were detached from the well plates after treatment with trypsin/EDTA solution (1.0 mL) and were washed with PBS. The cells were then incubated in the dark with 5.0µM dichlorodihydrofluorescein diacetate (DCF-DA, Invitrogen) for 30 min at 37 °C and immediately analysed by fluorescence-activated cell sorting (FACS) (FACSaria I, Becton Dickinson, San Jose, CA).

#### Western blot analysis

Each type of CDG and *f*-CDG thin film was placed on a 12-well cell culture plate (Corning Inc.) and washed with PBS. HeLa cells at 2x10<sup>4</sup> per well were cultured for 48 h in 5% CO<sub>2</sub> at 37 °C. After 48 h, the cells were washed twice with PBS and treated with 0.25% trypsin-EDTA solution for 5 min for detachment. Detached cells were centrifuged at 10,000 x g for 15 min. Collected cells were lysed in radio-immunoprecipitation assay (RIPA) buffer (20 mM Tris-HCl, pH 7.5, 150 mM NaCl, 1.0 mM Na<sub>2</sub>EDTA, 1.0 mM EGTA, 1% NP-40, 1% sodium deoxycholate, 2.5 mM sodium pyrophosphate, 1.0 mM-glycerophosphate, and protease inhibitor cocktail).

A total of 20 µg cell lysate was loaded and analysed by SDS-PAGE and blotted onto nitrocellulose membrane (Millipore). The blots were incubated with anti-vinculin ( $\alpha$ -vinculin) antibody (Cell Signalling Technology) overnight in a cold room. After incubation with primary antibodies, the membranes were washed in triplicate with TBST buffer (Tris-buffered saline-Tween 20) and incubated in horseradish peroxidase-conjugated secondary antibodies for 3 h at room temperature. Bands were detected using the SuperSignal West Pico Chemiluminescent Substrate kit (Thermo Scientific) according to the manufacturer's instructions.

#### Analysis of cell proliferation and viability

Cell proliferation was quantified using WST-1 assays (Takara Biomedical) by measuring the metabolic activities of viable cells. HeLa cells were briefly plated on CDG and *f*-CDG thin films in a 24-well plate and cultured for two days. Then, these cells were mixed with WST-1 solution (0.1mL) in 1.0 mL of growth medium and incubated for 3 h at 37 °C with 5% CO<sub>2</sub> in a humidified atmosphere. An aliquot of 110 µL was transferred into a 96-well plate, and absorbance was measured with a microplate reader (Bio-Rad) at 440 nm. Separately, absorbance at 690 nm was also measured as a reference using a spectrophotometer (SpectraMax M5, Molecular Devices). Each experiment was performed in triplicate, and the measured data

are shown with standard deviations. Student's t-test was used to analyse the relationships between the different variables.

### Statistical analysis

The data is expressed in terms of mean  $\pm$  standard deviation values. The student t-test was used to analyse the relationship between the different variables. A  $p$  value  $< 0.05$  was considered statistically significant.

### Conclusion

To improve the properties of Gr materials for biomedical applications, we studied the effects of CDG film nitrogen-functionalisation on biocompatibility. Nitrogen-containing functional groups were formed on CDG films by varying the time of  $N_2$  plasma treatment without the generation of plasma-induced defects. We investigated ROS generation, mitochondrial morphology, focal adhesion, cell shape, proliferation and viability for HeLa cells grown on CDG and  $f$ -CDG thin films. The ROS generation was decreased for cells grown on the  $f$ -CDG (20 s) films compared to those grown on the CDG and  $f$ -CDG (100 s) films. Cell shape, focal adhesion, proliferation and viability of HeLa cells grown on the  $f$ -CDG (20 s) film were significantly improved compared to those of the cells grown on CDG and  $f$ -CDG (100 s) films. The results also imply that an optimum condition exists for greater biocompatibility of functionalised CDG thin films as scaffolding materials. The modified surface characteristics generated by the N-containing functional groups improved biocompatibility of the CDG thin films, which enable the improvement and application of Gr materials to biomedical fields.

**Acknowledgments.** The Basic Science Research Program (Grant No. 2009-0083540, 2009-0093817 and 2012R1A1A3008822) through the National Research Foundation of Korea (NRF) funded by the Ministry of Education, Science and Technology (MEST), Korea supported this research.

### Notes and references

<sup>a</sup>School of Advanced Materials Science and Engineering, Center for Advanced Plasma Surface Technology and Center for Human Interface Nanotechnology, Sungkyunkwan University (SKKU), Suwon, Kyunggi-do 440-746, Korea. Fax: +82-31-290-7410; Tel: +82-31-290-7398; E-mail: nelee@skku.edu (N.-E. Lee)

<sup>b</sup>Samsung Advanced Institute for Health Sciences and Technology (SAIHST), Sungkyunkwan University (SKKU), Suwon, Kyunggi-do 440-746, Korea

<sup>c</sup>SKKU Advanced Institute of Nanotechnology (SAINT), Sungkyunkwan University (SKKU), Suwon, Kyunggi-do 440-746, Korea

<sup>d</sup>Department of Chemistry, Institute of Innovative Functional Imaging, Chung-Ang University, Seoul 156-756, Korea

† Electronic Supplementary Information (ESI) available: Experimental details, Table S1 and Fig. S1. See DOI: 10.1039/b000000x/

‡ Ok Ja Yoon and Chang Yong Jung contributed equally to this work.

- 1 Y. Wang, Z. Li, J. Wang, J. Li and Y. Lin, *Trends Biotechnol.*, 2011, **29**, 205-212.
- 2 H. Shen, L. Zhang, M. Liu and Z. Zhang, *Theranostics*, 2012, **2**, 283-294.
- 3 Y. Yang, A. M. Asiri, Z. Tang, D. Duand Y. Lin, *Mater. Today*, 2013, **16**, 365-373.

- 4 S.-R. Ryoo, Y.-K. Kim, M.-H. Kim and D.-H. Min, *ASC Nano*, 2010, **4**, 6587-659.
- 5 J. Shen, Y. Zhu, X. Yang and C. Li, *Chem. Comm.*, 2012, **48**, 3696-3699.
- 6 M. Nurunnabi, Z. Khatun, K. M. Huh and S. Y. Park, D. Y. Lee, K. J. Cho and Y.-k. Lee, *ACS Nano*, 2013, **7**, 6858-6867.
- 7 L. Feng, L. Wu and X. Qu, *Adv. Mater.*, 2013, **25**, 168-186.
- 8 K.-H. Liao, Y.-S. Lin, C. W. Macosko and C. L. Haynes, *ACS Appl. Mater. Interfaces*, 2011, **3**, 2607-2615.
- 9 N. Li, Q. Zhang, S. Gao, Q. Song, R. Huang, L. Wang, L. Liu, J. Dai, M. Tang and G. Cheng, *Scientific Reports*, 2013, **3**, 1-6.
- 10 S. Goenka, V. Sant and S. Sant, *J. Control. Release*, 2014, **173**, 75-88.
- 11 O. J. Yoon, C. Y. Jung, I. Y. Sohn, H. J. Kim, B. Hong, M. S. Jhon and N.-E. Lee, *Composites: Part A*, 2011, **42**, 1978-1984.
- 12 J. Liu and L. Cui, D. Losic, *Acta Biomater.*, 2013, **9**, 9243-9257.
- 13 B. Wang, P. G. Luo, K. N. Tackett II, O. N. Ruiz, C. E. Bunker, S. H. Cheng, A. Parenzan, and Y.-P. Sun, *J. Nanomater. Mol. Nanotechnol.*, 2012, **1**, 1-4.
- 14 C. Shan, H. Yang, D. Han, Q. Zhang, A. Ivaska and L. Niu, *Langmuir*, 2009, **25**, 12030-12033.
- 15 H. Fan, L. Wang, K. Zhao, N. Li, Z. Shi, Z. Ge and Z. Jin, *Biomacromolecules*, 2010, **11**, 2345-2351.
- 16 Y.-K. Kim, M.-H. Kim and D.-H. Min, *Chem. Commun.*, 2011, **47**, 3195-3197.
- 17 C. Fisher, A. E. Rider, Z. J. Han, S. Kumar, I. Levchenko, K. (Ken) Ostrikov, *J. Nanomater.*, 2012, **2012**, 1-19.
- 18 C. T. Laurencin, N. S. Nair, CRC Press, Taylor & Franch Group, 2008, pp171-178.
- 19 G. Y. Tonga, K. Saha and V. M. Rotello, *Adv. Mater.*, 2014, **26**, 359-370.
- 20 F. F. Borghi, A. E. Rider, S. Kumar, Z. J. Han, D. Haylock and K. Ostrikov, *J. Nanomater.*, 2013, **2013**, 1-15.
- 21 M. E. Demirbilek, M. Demirbilek, Z. Karahalioglu, E. Erdal, T. Vural, E. Yalçın, N. Sağlam, E. B. Denkbaş, *Appl. Biochem. Biotechnol.*, 2011, **164**, 780-792.
- 22 O. J. Yoon, H. J. Lee, Y. M. Jang, H. W. Kim, W. B. Lee, S. S. Kim and N.-E. Lee, *Appl. Surf. Sci.*, 2011, **257**, 8535-8541.
- 23 H. J. Lee, J. Park, O. J. Yoon, H. W. Kim, D. Y. Lee, D. H. Kim, W. B. Lee, N.-E. Lee, J. V. Bonventre and S. S. Kim, *Nat. Nanotechnol.*, 2011, **6**, 121-125.
- 24 S. Marchi, C. Giorgi, J. M. Suski, C. Agnoletto, A. Bononi, M. Bonora, E. D. Marchi, S. Missiroli, S. Patergnani, F. Poletti, A. Rimessi, J. Duszynski, M. R. Wieckowski, and P. Pinton, *J. Sig. Transd.*, 2012, **2012**, 1-17.
- 25 D. Trachootham, W. Lu, M. A. Ogasawara, N. R.-D. Valle and P. Huang, *Antioxid. Redox. Sig.*, 2008, **10**, 1343-1374.
- 26 R. S. Bhimani, W. Troll, D. Grunberger and K. Frenkel, *Cancer Research*, 1993, **53**, 4528-4533.
- 27 T. P. A. Devasagayam, J. C. Tilak, K. K. Bloor, K. S. Sane, S. S. Ghaskadbi and R. D. Lele, *J. Assoc. Physicians India*, 2004, **52**, 794-796.
- 28 M. P. Murphy, *Biochem. J.*, 2009, **417**, 1-13.
- 29 D. Wei, Y. Liu, Y. Wang, H. Zhang, L. Huang and G. Yu, *Nano Lett.*, 2009, **9**, 1752-1758.
- 30 H. Wang, T. Maiyalagan and X. Wang, *ACS Catal.*, 2012, **2**, 781-794.
- 31 Y. Wang, Y. Shao, D. W. Matson, J. Lin, Y. Lin, *ACS NANO*, 2010, **4**, 1790-1798.
- 32 K. Burrige, K. Fath, T. Kelly, G. Nuckolls and C. Turner, *Annu. Rev. Cell Biol.*, 1988, **4**, 487-525
- 33 R. M. Ezzell, W. H. Goldmann, N. Wang, N. Parasharama and D. E. Ingber, *Exp. Cell Res.*, 1997, **231**, 14-26.
- 34 A. Byron, J. D. Humphries, J. A. Askari, S. E. Craig, A. P. Mould and M. J. Humphries, *J. Cell Sci.*, 2009, **122**, 4009-4011.
- 35 C. Perier and M. Vila, *Cold Spring Harb. Perspect. Med.*, 2012, **2**, 1-19.
- 36 N. Arakaki, T. Nishihama, H. Owaki, Y. Kuramoto, M. Suenaga, E. Miyoshi, Y. Emoto, H. Shibata, M. Shono and T. Higuti, *Biol. Pharm. Bull.*, 2006, **29**, 1962-1965.

- 
- 37 S. Lee, S. Kim, X. Sun, J.-H. Lee, H. Cho, *Biochem. Biophys. Res. Commun.*, 2007, **357**, 111-117.
- 38 B. Westermann, *Nature*, 2010, **11**, 872-884.
- 39 Y. Chang, S.-T. Yang, J.-H. Liu, E. Dong, Y. Wang, A. Cao, Y. Liu,  
5 H. Wang, *Toxicol. Lett.*, 2011, **200**, 201-210.
- 40 N. J. Hallab, K. J. Bundy, K. O'Connor, R. L. Moses, J. J. Jacobs,  
*Tissue Eng.*, 2001, **7**, 55-71.